Materials Science & Engineering A 818 (2021) 141425

Contents lists available at ScienceDirect

Materials Science & Engineering A

journal homepage: www.elsevier.com/locate/msea

Short communication

Solid state welding of medium-entropy CrCoNi with heterogeneous, partially recrystallized microstructures

C.E. Slone [a,b,*], B. Barnett [b], B. Georgin [a,b], A. Vivek [b], E.P. George [c,d], G.S. Daehn [b], M.J. Mills [a,b]

[a] Center for Electron Microscopy and Analysis, The Ohio State University, Columbus, OH, 43212, USA
[b] Department of Materials Science and Engineering, The Ohio State University, Columbus, OH, 43210, USA
[c] Materials Science and Technology Division, Oak Ridge National Laboratory, Oak Ridge, TN, 37831, USA
[d] Materials Science and Engineering Department, University of Tennessee, Knoxville, TN, 37996, USA

ARTICLE INFO

Keywords:
Medium- and high-entropy alloys
Partially recrystallized microstructures
Ultra-high strength
Collision welding
Solid state joining

ABSTRACT

Heterogeneous, partially recrystallized (PRX) microstructures have recently been used to improve strength-ductility combinations in high-entropy alloys. However, these microstructures are incompatible with conventional joining processes that require melting or prolonged exposure to elevated temperatures. This work presents an initial exploration of solid state joining in this challenging condition using vaporizing foil actuator welding (VFAW) applied to PRX equiatomic alloy CrCoNi.

1. Introduction

Single-phase high- and medium-entropy alloys (HEAs, MEAs) such as the equiatomic CrMnFeCoNi or CrCoNi systems have been recognized for their outstanding ductility, fracture toughness, and high work hardening rates [1–3], but recent work has focused on enhancing their modest yield strengths through thermomechanical processing. Cold-rolling and annealing to produce a partially recrystallized (PRX) microstructure has been shown to enhance the yield strength while preserving acceptable ductility in CrCoNi [4,5], CrMnFeCoNi [6], and (Cr,Co)-rich commercial Ni-base alloy Inconel 740H [7]. High work hardening rates and the success of the PRX strategy are apparently the product of low stacking fault energies, which promote deformation twinning and in some cases deformation-induced phase transformations.

Despite these encouraging improvements in yield strength, the PRX alloys are likely to be incompatible with conventional joining techniques. High yield strengths in these alloys depend intimately on microstructural features generated during prior deformation (e.g., deformation twins, twin/ε-martensite lamellae, and dislocation locks). Exposure to elevated temperatures results in recrystallization of the material, which can begin above approximately 580 °C for heavily cold-rolled CrCoNi [5]. In conventional welding processes, recrystallization in the heat-affected zone and full melting and re-solidification of the weld metal eliminates the carefully engineered PRX microstructures described in recent publications. It is imperative to examine alternative joining techniques if these ultra-high strength materials will be considered for industrial applications. To the authors' knowledge, no studies have been performed to assess whether PRX microstructures can be retained after joining.

Significant progress has recently been made in developing solid-state joining methods that dramatically reduce thermal input and do not require melting of the base components. Although friction stir welding is the most prominent example [8], the vaporizing foil actuator welding (VFAW) method has also been used to join strong, dissimilar alloys with heat-sensitive microstructures [9–11]. VFAW forms metallurgical bonds using high-velocity impacts between workpieces and imparts substantial deformation and jetting off the nascent surface near the bond line. In addition, such shocks can be used for surface modification, similar to laser shock, or shot peening. For example, the vaporizing foil actuator technique was used to develop a shock wave to introduce extreme twinning and surface hardening in austenitic stainless steel 316L [12]. The potential benefits of the technique for PRX alloys are clear: not only is heat input minimal, but additional deformation imparted at the bond line may make the weld stronger than the PRX base metal. VFAW is typically used with foil or thin sheet flyer plates up to 10 mm which can be joined to targets of arbitrary thickness. Vaporizing Foil Actuators (VFA's) can also be used to generate impulse for numerous other manufacturing techniques such as tube and flange welding, as well as forming, shearing, and embossing of thin sheets [9].

This work explores the use of VFAW to join partially recrystallized,

* Corresponding author. Materials and Corrosion Engineering Practice, Exponent, Inc., 149 Commonwealth Drive, Menlo Park, CA 94025, USA.
E-mail address: cslone@exponent.com (C.E. Slone).

https://doi.org/10.1016/j.msea.2021.141425
Received 6 January 2021; Received in revised form 4 May 2021; Accepted 5 May 2021
Available online 8 May 2021
0921-5093/

equiatomic CrCoNi. The microstructure and tensile properties of this condition have previously been reported [5], and it exhibits outstanding combinations of tensile yield strength and ductility. In this study, the amenability of PRX microstructures to undergo solid-state joining is assessed for the first time.

2. Materials and methods

For this work, equiatomic CrCoNi alloy was cast, homogenized under vacuum at 1200 °C for 24 h, cold-rolled to 70% reduction in thickness, and annealed in air at 600 °C/1 h. Additional processing details and the microstructure and tensile properties of this condition have previously been reported [5]. In the previous work, this produced a recrystallized area fraction of 39%, yield strength of 1112 MPa, ultimate tensile strength of 1269 MPa (engineering stress) or 1336 MPa (true stress), and total elongation of 23%.

The setup for VFAW is shown in Fig. 1 and has been described in detail by Vivek et al. [13]. In summary, a metallurgical bond is formed between two components with one component designated as the "target" and the other designated as the "flyer". The target remains stationary while an intense, pulsed current is passed through an aluminum foil, which vaporizes and propels the flyer into the target at high velocity. For this work, coupons of PRX CrCoNi were prepared by electrical discharge machining with dimensions of approximately 10 mm (width) x 25 mm (length) x 0.8 mm (thickness) and used as both target and flyer. EDM and oxide layers on the joining faces were removed using 240, 400, and 600-grit silicon carbide paper. Welds were produced using aluminum foil actuators with thickness 0.0762 mm, and a Maxwell Magneform capacitor bank system, which discharged 4 kJ over a nominal short-circuit rise time of 12 μs. The standoff distance between the flyer and target (illustrated in Fig. 1) was 1.6 mm and standoff sheets were separated by an in-plane distance of 6.15 mm. Photonic Doppler velocimetry [14] measured a flyer velocity of approximately 0.432 km/s, corresponding to kinetic energy on impact of approximately 1.18 kJ. Metallographic analysis was performed on one sectioned weld coupon using a Thermofisher Scientific Apreo scanning electron microscope (SEM), with electron-backscatter diffraction (EBSD) performed using TSL OIM 8 software [15]. Three additional specimens were subjected to peel testing using an MTS 810 mechanical testing frame at a cross-head speed of 0.0166 mm/s until specimen failure. As shown in Fig. 1, VFAW welds characteristically have small unbonded areas at the center of the bond line.

3. Results

The microstructure produced by VFAW is shown in Fig. 2. Fig. 2a shows a schematic representation of the flyer and target after joining. The bond interface had a predominantly wavy structure, which is characteristic of impact welds [16]. At the center of the joint, the interface was flat (and presumably unbonded) over about 2% of the total interface length. Fig. 2b shows a low-magnification SEM image of the wavy structure, which had wavelengths between approximately 30–60 μm.

Fig. 2c through 2f show the microstructure at the bond line in greater detail. As noted previously, the initial (pre-welding) microstructures of both the flyers and targets were partially recrystallized. Previous work has shown that non-recrystallized grains retain high dislocation densities and deformation twins, in contrast to very low dislocation densities in recrystallized grains [17]. At distances from the bond line of about 20 μm or greater, this base microstructure (Zone 1 in Fig. 2c–e) was visually unaffected by welding, which suggests a much smaller process zone than in conventional fusion welds with heat-affected zone widths on the order of millimeters [18].

Aside from the base PRX microstructure (Zone 1), three additional zones were observed following the welding process (Zones 2, 3, and 4). Zone 2, which had a typical width of approximately 10 μm, occurred on each side of the bond line and was severely deformed. As shown in the EBSD inverse pole map of Fig. 2c, plastic deformation was too extreme to index the crystallographic orientations in this zone. Manual examination of corresponding electron backscatter diffraction patterns from Zone 2 indicated that no visually discernible patterns were produced, likely due to extreme refinement of the deformation substructure and overlapping crystal orientations at length scales below the spatial resolution of the technique.

The remaining Zones 3 and 4 contained two distinct populations of recrystallized grains with different size distributions. Zone 3 contained relatively coarse elongated grains with sizes on the order of 1 μm. These were non-equiaxed and typically perpendicular to the curved bond line. These features are consistent with a re-solidified structure, which is often seen in isolated pockets in impact welds. Although a minimum velocity must be achieved to produce a robust metallurgical bond, future optimization may include using less energy to eliminate the relatively coarse recrystallized grains.

In contrast to Zone 3, the grains in Zone 4 were much finer and did not exhibit any apparent preferred growth direction relative to the bond line. Similar nanocrystalline regions have previously been observed in dissimilar metal VFAW between aluminum alloy 6111-T4 and DP980 steel [11]. This was attributed to deformation-induced dynamic recrystallization, which has also been observed following other modes of severe plastic deformation [19]. As estimated from EBSD measurements, the nanocrystalline grains in Zone 4 had typical sizes on the order of 10–100 nm with the largest grains reaching sizes up to about 500 nm.

Peel testing of the sectioned, welded coupons indicated strengths of approximately 60–100 N/mm (applied load P divided by specimen width w). A photograph taken during peel testing is shown in Fig. 3a with test results shown in Fig. 3b. Variability in the tests was caused predominantly by disparities in sample geometry and incomplete bonding on some parts of the welds. Peel strengths are typically reported

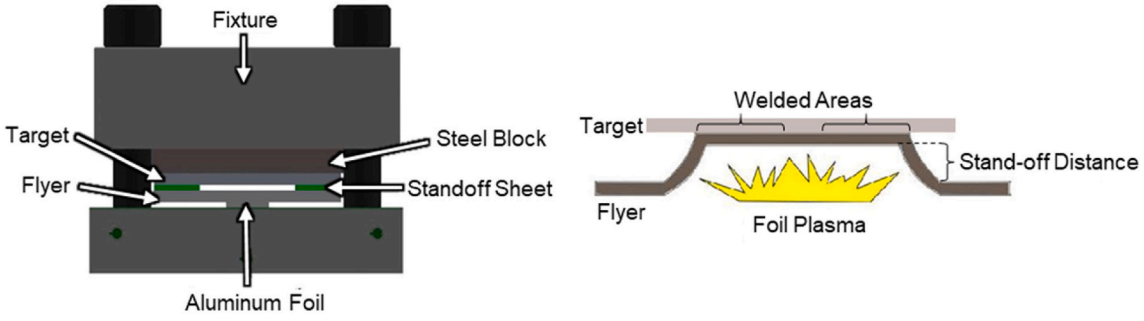

Fig. 1. Schematic representation of the VFAW process. The target and flyer, both PRX CrCoNi, are initially separated by the stand-off distance. A pulsed current vaporizes the aluminum foil and the resulting pressure propels the flyer into the target at high velocities, resulting in a solid-state weld between the two coupons of PRX CrCoNi.

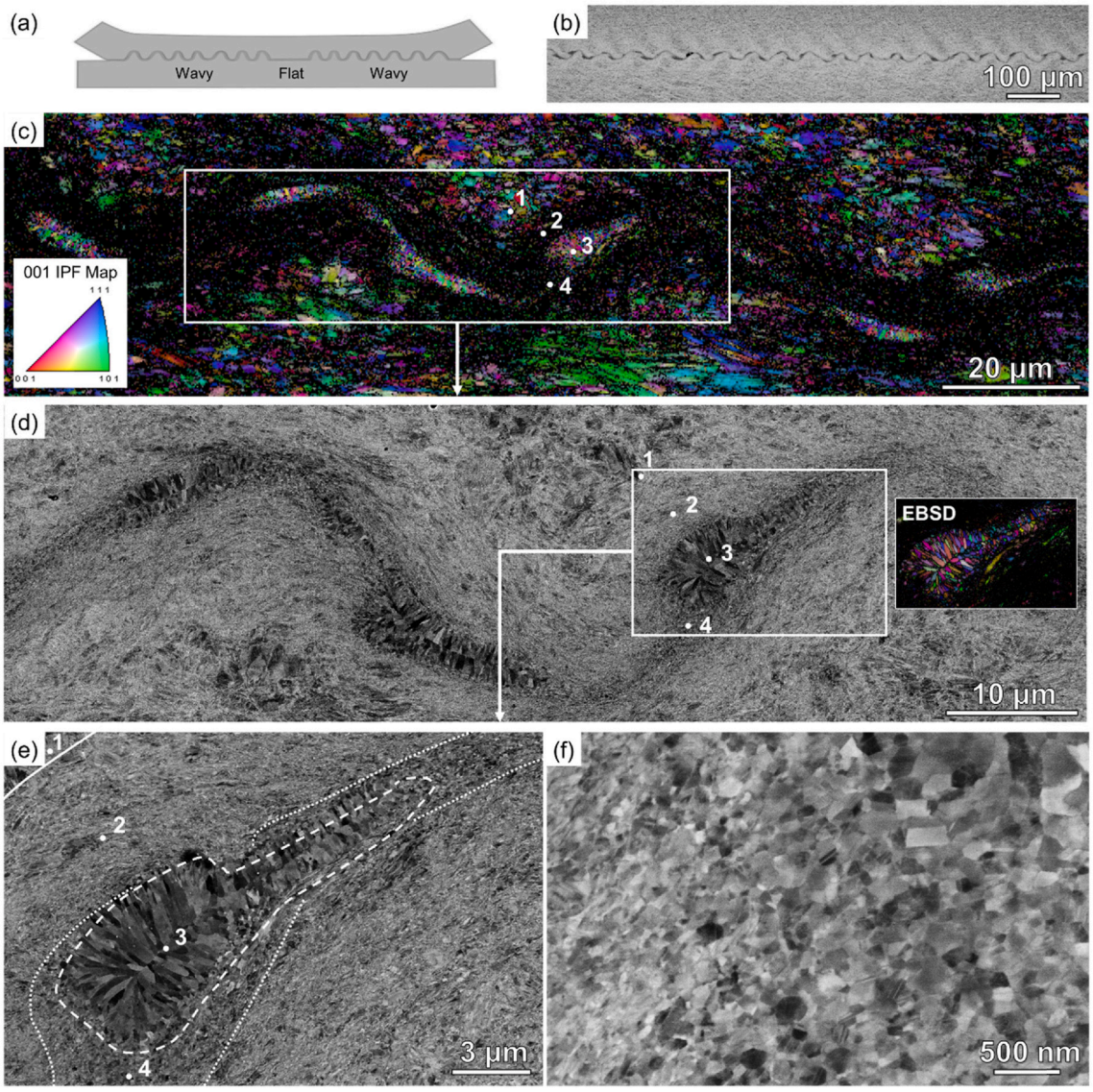

Fig. 2. Microstructure of a VFA weld between PRX CrCoNi coupons. (a) Schematic representation of the weld joint. The interface is wavy on both ends with a small flat region in the center. (b) SEM image of the wavy interface. (c) EBSD inverse pole figure map showing four distinct microstructural zones described in the text. (d) and (e) SEM-BSE overview images of the four distinct microstructural zones. (f) Nano-scale recrystallized grains in Zone 4.

as units of force divided by specimen width (e.g., N/mm) because the specimen geometry produces a sharp crack-like feature that spans the width of the test coupon. Further, the stress is highest near the tip of the crack-like feature. The welded areas on each coupon were estimated from optical micrographs after testing to calculate the peel stress (N/mm^2). When normalized by the total area of welded material, the apparent scatter in the load-displacement curves is substantially reduced (Fig. 3b, inset). The peel stress values cannot be compared to values obtained by uniaxial tensile testing because the load is not uniformly distributed over the cross section.

The load-displacement curves exhibited signatures consistent with stable ductile tearing through the duration of the test, including one case where stable tearing appeared after a crack "pop-in" and subsequent crack arrest, as shown in Fig. 3b. No load-displacement signatures consistent with brittle failure were observed, and the samples' load response demonstrated significant plastic yielding prior to the onset of interface tearing. These observations support the hypothesis that as-welded VFAW welds retained many of the mechanical property benefits of the base material and avoid the interfacial strength debits common in traditional fusion weld interfaces.

Fracture surfaces following peel testing are shown in Fig. 4. Failure predominantly occurred by micro-void coalescence, which is a ductile fracture mode. Fig. 4a and b also show periodic variations in surface topography consistent with the wavy interface shown in Fig. 2b. This suggests failure occurred along the bond line. In some locations, micro-voids were much finer and only visible at high magnification, which likely reflects the nano-scale recrystallized grains in Zone 4 of the weld. A faceted second phase was observed in some rupture dimples (Fig. 4c and d). SEM energy-dispersive X-ray spectroscopy identified chromium and oxygen enrichment in these particles, which were also visible in the as-welded profile prior to testing (Fig. 4e). The presence of these secondary phases at the fracture surface indicate they may play a role in failure initiation, although this may be conflated with lower local strength due to the presence of coarse recrystallized grains along the bond line.

4. Discussion

The good strength/ductility combination of the welded PRX material may originate from composite-like behavior that has previously been

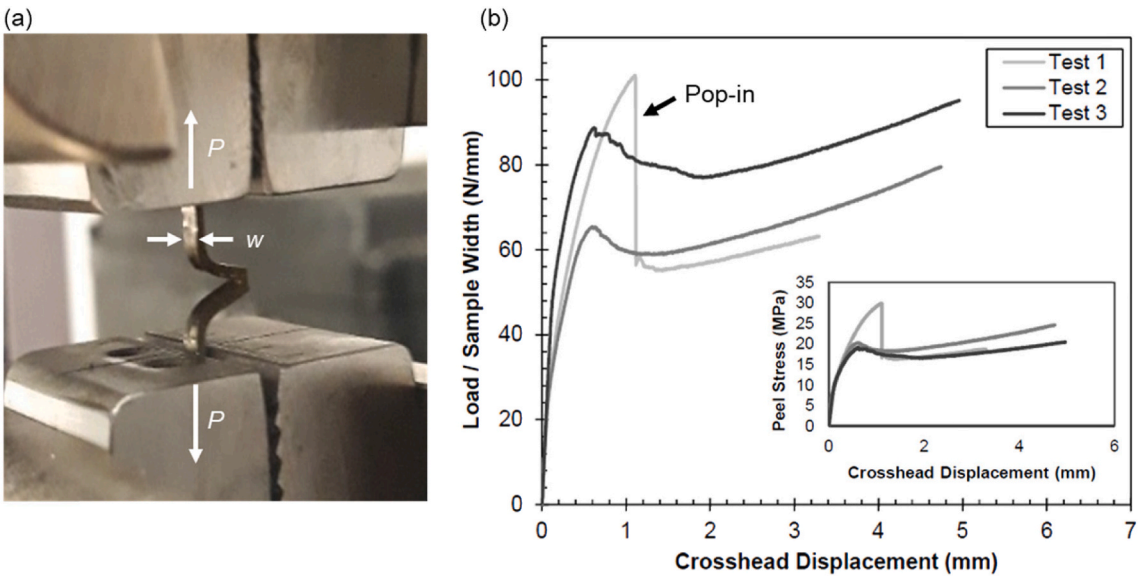

Fig. 3. (a) Snapshot during peel testing of a welded coupon. (b) Load-displacement results from peel testing. Inset: Load normalized by the weld area measured after peel testing.

demonstrated by the PRX base metal. Slone et al. have shown that non-RX grains behave like hard inclusions in a relatively soft matrix of fine RX grains. This generates a composite-like response despite its uniform composition and single-phase condition [5]. For the welded material in this work, the process zone around the bond line consists of a continuous boundary layer of extremely hard grains (Zone 2) surrounding softer recrystallized grains (Zones 3 and 4). Although the hardness was not directly measured in these areas, the relative hardness is known based on the degree of deformation and work hardening, which was qualitatively assessed from EBSD measurements. The nanocrystalline grains in Zone 4 may also have significantly elevated strength due to the Hall-Petch effect. The wavy morphology of the interface may strengthen the weld in Mode I or Mode II loading, since layered RX and non-RX grains would be oriented perpendicular to the crack-opening or shearing direction. Furthermore, it is expected that other extrinsic toughening mechanisms may enhance the ability of the CrCoNi alloy to withstand fracture, such as nano-twin crack bridging that has been reported in the equiatomic CrMnFeCoNi alloy [20].

It should also be noted that local strength in Zone 2, which was even more severely deformed than the base metal, is expected to be exceptionally high. This follows from the extreme refinement of the deformed microstructure via mechanical twinning, twin/ε-martensite lamellae, and other dislocation locks. As previously demonstrated in stainless steel alloy 316L, there may also be an opportunity to use the VFAW technique with lower input energies to shock harden the alloy surface [12].

Crack initiation during peel testing may have occurred at hard, brittle chromium oxide particles at the bond line. Although some oxide particles were sparsely distributed through the base PRX metal, the oxides at the bond line were surrounded by recrystallized material and most likely formed during welding. During impact between the flyer and target, a solid jet is developed that removes the external surface and can throw hot fragmented metal outward in front of the contact point. This jetting may rapidly produce an oxide that ejects and is deposited in the soon-to-be-bonded surface. This is a possible explanation for the entrained chromia particles. Welding in an inert gas environment may mitigate this effect. Additionally, reducing the input energy, velocity of the flyer, and heat generated on impact may minimize the degree of melting and recrystallization at the bond line, further strengthening the welds.

5. Conclusions

In summary, this work presents the first demonstration of a solid-state joining technique on a multi-principal element alloy with a heterogeneous partially recrystallized (PRX) microstructure. Use of vaporizing foil actuator welding produced robust metallurgical bonds without inducing widespread recrystallization of the base metal. Three distinct regions around the bond line were identified in addition to the base metal. The entire process zone exhibited total widths on the order of approximately 40 μm, which is much finer than heat affected zones in conventional welding processes. Peel testing showed ductile fracture indications along the bond line with initiation possibly occurring at chromium oxide particles formed during welding. This work provides broadly applicable insights regarding microstructural features in the process zone of VFAW welds and indicates that heterogeneous, PRX alloys may be metallurgically joined using solid-state methods.

Data availability

The raw/processed data required to reproduce these findings cannot be shared at this time due to technical or time limitations.

I write on behalf of myself and all co-authors to confirm that the results reported in the manuscript are original and neither the entire work, nor any of its parts have been previously published. The authors confirm that the article has not been submitted to peer review, nor has been accepted for publishing in another journal. The author(s) confirms that the research in their work is original, and that all the data given in the article are real and authentic. If necessary, the article can be recalled, and errors corrected.

CRediT authorship contribution statement

C.E. Slone: Conceptualization, Investigation, Writing – original draft, Writing – review & editing, Visualization. **B. Barnett:** Conceptualization, Investigation, Writing – review & editing. **B. Georgin:** Investigation, Writing – review & editing. **A. Vivek:** Conceptualization. **E.P. George:** Supervision. **G.S. Daehn:** Conceptualization, Writing – review & editing, Supervision, Funding acquisition. **M.J. Mills:** Conceptualization, Writing – review & editing, Supervision, Funding acquisition.

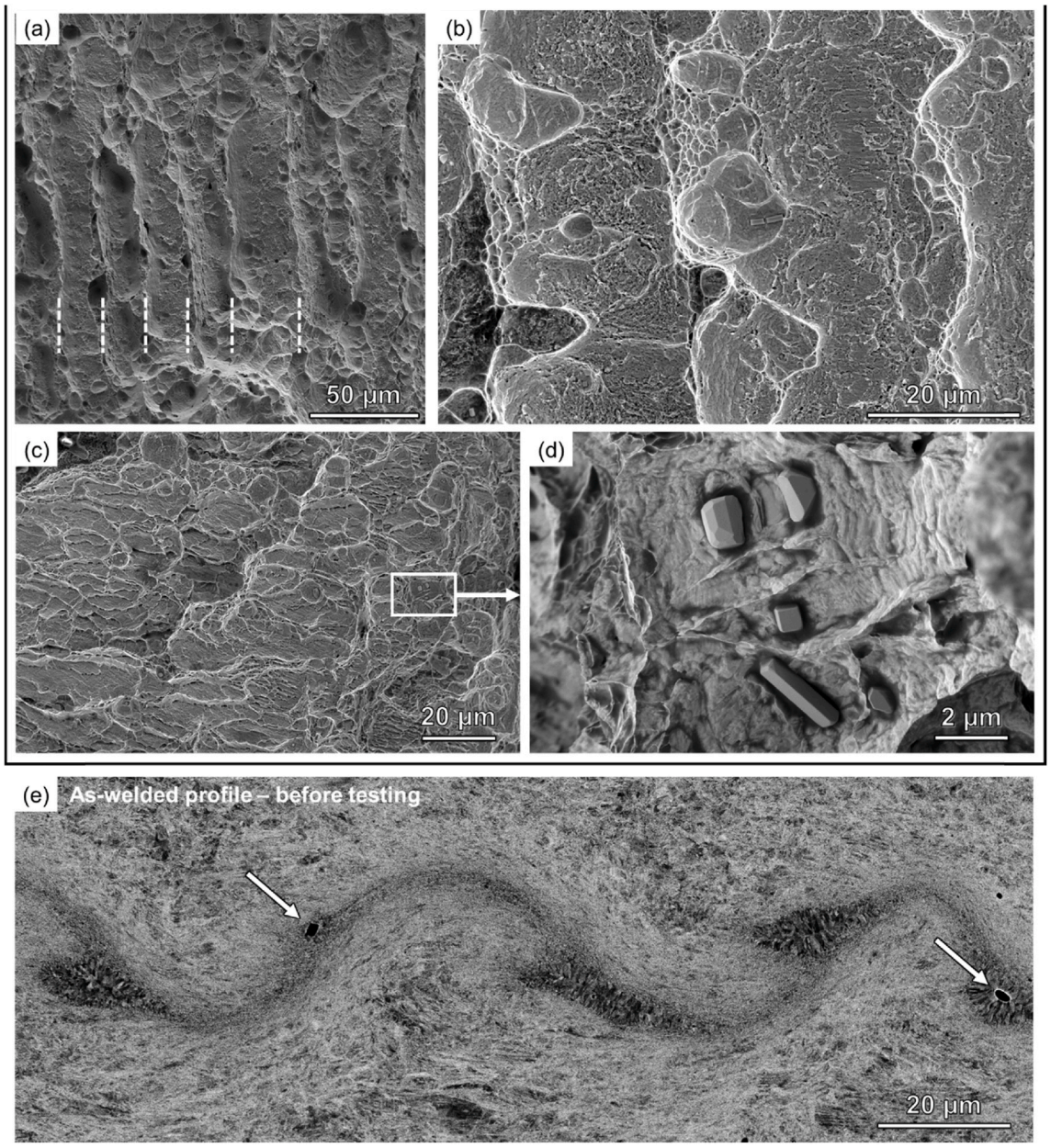

Fig. 4. (a–d) Fracture surfaces following peel testing. (a) Secondary electron SEM image shows parallel linear features with periodic spacing consistent with the wavelength of the as-welded interface shown in Fig. 2b. (b) Parallel features at higher magnification showing ductile micro-voids. (c,d) Additional microvoids with (Cr,O)-rich particles. (e) White arrows indicate corresponding particles in the as-welded microstructure prior to testing.

Declaration of competing interest

The authors declare that they have no known competing financial interests or personal relationships that could have appeared to influence the work reported in this paper.

Acknowledgments

The National Science Foundation, Division of Materials Research is acknowledged for supporting CES and MJM (thermo-mechanical processing and materials characterization) under contract DMR-1508505 and DMR-1905748. CES was also supported by the National Science Foundation Graduate Research Fellowship Program Grant No. DGE-1343012. Any opinions, findings, and conclusions or recommendations expressed in this material are those of the authors and do not necessarily reflect the views of the National Science Foundation. BB, AV, and GSD (dynamic materials processing and testing) were supported by NSF Major Research Instrumentation Award CMMI-1531785. BG (materials characterization) was supported by the Center for Accelerated Maturation of Materials (CAMM). EPG (materials synthesis) is supported by the U.S. Department of Energy, Office of Science, Basic Energy Sciences, Materials Sciences and Engineering Division.

References

[1] A. Gali, E.P. George, Tensile properties of high- and medium-entropy alloys, Intermetallics 39 (2013) 74–78, https://doi.org/10.1016/j.intermet.2013.03.018.
[2] B. Gludovatz, A. Hohenwarter, D. Catoor, E.H. Chang, E.P. George, R.O. Ritchie, A fracture-resistant high-entropy alloy for cryogenic applications, Science 345 (80) (2014) 1153–1158, https://doi.org/10.1126/science.1254581.
[3] B. Gludovatz, A. Hohenwarter, K.V.S. Thurston, H. Bei, Z. Wu, E.P. George, R. O. Ritchie, Exceptional damage-tolerance of a medium-entropy alloy CrCoNi at cryogenic temperatures, Nat. Commun. 7 (2016) 10602, https://doi.org/10.1038/ncomms10602.

[4] M. Yang, D. Yan, F. Yuan, P. Jiang, E. Ma, X. Wu, Dynamically reinforced heterogeneous grain structure prolongs ductility in a medium-entropy alloy with gigapascal yield strength (SUPPLEMENTARY INFORMATION), Proc. Natl. Acad. Sci. Unit. States Am. (2018), https://doi.org/10.1073/pnas.
[5] Achieving ultra-high strength and ductility in equiatomic CrCoNi with partially recrystallized microstructures, Acta Mater. 165 (2019) 496–507, https://doi.org/10.1016/j.actamat.2018.12.015.
[6] C. Haase, L.A. Barrales-Mora, Influence of deformation and annealing twinning on the microstructure and texture evolution of face-centered cubic high-entropy alloys, Acta Mater. 150 (2018) 88–103, https://doi.org/10.1016/j.actamat.2018.02.048.
[7] C.E. Slone, J. Miao, M.J. Mills, Ultra-high strength and ductility from rolling and annealing of a Ni-Cr-Co superalloy, Scripta Mater. 155 (2018), https://doi.org/10.1016/j.scriptamat.2018.06.033.
[8] R. Nandan, T. DebRoy, H.K.D.H. Bhadeshia, Recent advances in friction-stir welding - process, weldment structure and properties, Prog. Mater. Sci. 53 (2008) 980–1023, https://doi.org/10.1016/j.pmatsci.2008.05.001.
[9] A. Vivek, G.A. Taber, J.R. Johnson, S.T. Woodward, G.S. Daehn, Electrically driven plasma via vaporization of metallic conductors: a tool for impulse metal working, J. Mater. Process. Technol. 213 (2013) 1311–1326, https://doi.org/10.1016/j.jmatprotec.2013.02.010.
[10] S. Chen, G.S. Daehn, A. Vivek, B. Liu, S.R. Hansen, J. Huang, S. Lin, Interfacial microstructures and mechanical property of vaporizing foil actuator welding of aluminum alloy to steel, Mater. Sci. Eng. 659 (2016) 12–21, https://doi.org/10.1016/j.msea.2016.02.040.
[11] B. Liu, A. Vivek, M. Presley, G.S. Daehn, Dissimilar impact welding of 6111-T4, 5052-H32 aluminum alloys to 22MnB5, DP980 steels and the structure–property relationship of a strongly bonded interface, Metall. Mater. Trans. A Phys. Metall. Mater. Sci. 49 (2018) 899–907, https://doi.org/10.1007/s11661-017-4429-7.
[12] A.K. Agrawal, A. Singh, A. Vivek, S. Hansen, G. Daehn, Extreme twinning and hardening of 316L from a scalable impact process, Mater. Lett. 225 (2018) 50–53, https://doi.org/10.1016/j.matlet.2018.04.044.
[13] A. Vivek, S.R. Hansen, B.C. Liu, G.S. Daehn, Vaporizing foil actuator: a tool for collision welding, J. Mater. Process. Technol. 213 (2013) 2304–2311, https://doi.org/10.1016/j.jmatprotec.2013.07.006.
[14] G.S. Daehn, Y. Zhang, S. Golowin, K. Banik, A. Vivek, J.R. Johnson, G. Taber, G. K. Fenton, I. Henchi, P. L'Eplattenier, Coupling experiment and simulation in electromagnetic forming using Photon Doppler Velocimetry, in: 3rd Int. Conf. High Speed Form, Dortmund, Germany, 2008, pp. 35–44, https://doi.org/10.2374/SRI08SP160.
[15] OIM Analysis, Version 8.0, 2016.
[16] T. Lee, S. Zhang, A. Vivek, G. Daehn, B. Kinsey, Wave formation in impact welding: study of the Cu–Ti system, CIRP Ann 68 (2019) 261–264, https://doi.org/10.1016/j.cirp.2019.04.058.
[17] C.E. Slone, J. Miao, E.P. George, M.J. Mills, Achieving ultra-high strength and ductility in equiatomic CrCoNi with partially recrystallized microstructures, Acta Mater. 165 (2019) 496–507, https://doi.org/10.1016/j.actamat.2018.12.015.
[18] J.C. Lippold, Welding Metallurgy and Weldability, John Wiley & Sons, Inc., Hoboken, New Jersey, 2015.
[19] U. Andrade, M.A. Meyers, K.S. Vecchio, A.H. Chokshi, Dynamic recrystallization in high-strain, high-strain-rate plastic deformation of copper, Acta Metall. Mater. 42 (1994) 3183–3195, https://doi.org/10.1016/0956-7151(94)90417-0.
[20] Z. Zhang, M.M. Mao, J. Wang, B. Gludovatz, Z. Zhang, S.X. Mao, E.P. George, Q. Yu, R.O. Ritchie, Nanoscale origins of the damage tolerance of the high-entropy alloy CrMnFeCoNi, Nat. Commun. 6 (2015) 10143, https://doi.org/10.1038/ncomms10143.